International Forum on Aeroelasticity and Structural Dynamics
IFASD 2024
17-21 June 2024, The Hague, The Netherlands

GUST ENCOUNTER OF A SUPERSONIC FIGHTER AIRCRAFT USING CFD METHODS

Arne Voß[1]

[1] DLR - German Aerospace Center
Institute of Aeroelasticity
Bunsenstr. 10, 37073 Göttingen, Germany
arne.voss@dlr.de

Keywords: Gust loads, closed-loop gust encounter, military fighter aircraft, CFD

Abstract: The gust encounter of a supersonic fighter aircraft is investigated with the CFD code SU2 and the aerodynamic panel methods VLM and ZONA51. The interaction of the elastic aircraft, the flight controller and the gust is captured in a closed-loop time domain simulation. The comparisons show a moderate agreement between aerodynamic panel methods and CFD in terms of section loads, which has multiple reasons: first, the two aerodynamic methods yield different pitching moment characteristics, which have an influence on the flight mechanical reaction of the aircraft and the reaction of the flight controller. Second, due to the increase of the effective angle of attack during the gust encounter, vortices develop, which are not present in the horizontal level flight condition. Because of the large suction peaks due to the vortices, the surface pressure distribution changes significantly, an effect that is missed completely by the aerodynamic panel methods. The section loads predicted by the CFD based approach are higher, which eventually influences the structural sizing of the aircraft. Also, there is a significant structural dynamic reaction, which shows that for fighter aircraft, a transient gust analysis including structural elasticity is essential for the aircraft design.

1 MOTIVATION AND INTRODUCTION

The structural design of supersonic fighter aircraft is typically driven by their high requirements on maneuverability and the correspondingly high maneuver loads. Because of that, the design of the DLR Future Fighter Demonstrator (FFD) was based on maneuver loads only [30]. In a second publication, the author explored if gusts can exert higher loads on the primary structure in terms of section loads and structural dynamic accelerations [29] using aerodynamic panel methods. In this work, the focus is on the comparison of the aerodynamic panel methods with CFD, taking CFD as a reference. Possible differences are due to the vortex dominated flow as well as different aerodynamic centers and pitching moments. Because the aircraft is designed to be longitudinally unstable in the subsonic regime, a flight controller becomes mandatory. Thus, the interaction of the elastic aircraft, the gust and the flight controller is captured in a closed-loop time domain simulation. This publication will

consider the aircraft as a whole (instead of focusing on one discipline only), which makes a distinction of different physical effects more difficult, but delivers more realistic results.

2 LITERATURE REVIEW AND METHODOLOGY

As of today, time-linearized CFD methods are state-of-the art for the analysis of gust loads in an industrial context, as shown for example by Weigold et al. [31], who presented the approach of Airbus. Vidy et al. [24,25] demonstrated the application of time-linearized CFD methods at Airbus Defense and Space for both the gust encounter and flutter analysis. Next to time-linearized CFD methods, a slightly different approach was presented by Quero Martin [21], who proposed a correction scheme for frequency domain aerodynamic panel methods, such as the doublet lattice method, with results obtained from CFD. However, the unsteady transonic flow about an airfoil can be non-linear with respect to the amplitude of the excitation, as shown by Friedewald [12]. With respect to the NASA Common Research Model, Friedewald found a limitation of the maximum lift during a gust encounter due to shock-induced flow separation, if the excitation is large enough [11]. Similar comparisons of time-linearized CFD methods with their non-linear counterpart in the time domain were performed by Bekemeyer [5,6], who also tried to capture the non-linear effects in a reduced order model. However, in these publications the airfoil or the aircraft were rigid and fixed, without any reaction of the aircraft to the gust. This was addressed by Kaiser et al. [14], who studied the nonlinear gust encounter of a free-flying, elastic passenger transport aircraft and showed that time-linearized CFD methods are not always conservative, as non-linear effects are not captured. In the transonic flow for example, not only the shock intensity increases depending on the gust amplitude and length, but the shock moves up and down in stream-wise direction. The authors demonstrated that the application of a time-linearized CFD method fails to capture the shock motion, and as the pressures are simply scaled by the gust amplitude, the method produces non-physical peaks in the pressure distribution.

Note that some publications report significant differences between CFD and aerodynamic panel methods at operational points and with simple geometries, for which the results should converge (e.g. rectangular wing in subsonic flow). Those publications are excluded from this literature overview.

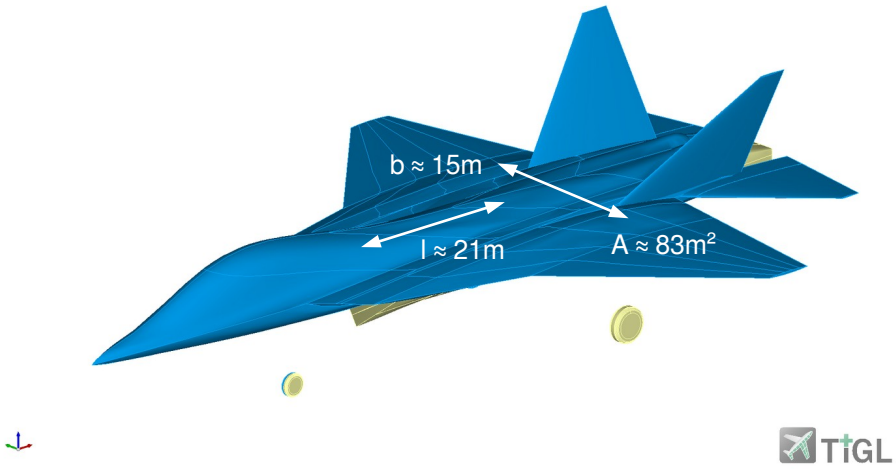

Figure 1: The DLR Future Fighter Demonstrator (FFD), CPACS file visualized in the TiGL Viewer

Also note that despite certain shortcomings, time-linearized CFD methods are suitable and necessary for efficient flutter analysis or continuous turbulence and are ideal for any application where existing transfer functions (GAFs) can be re-combined, for example to assess different mass configurations. Also, using a transfer function based approach allows to directly identify the contribution of a mode shape to a certain physical effect.

Looking at the gust encounter of fighter aircraft, Becker [4] (Messerschmitt-Bölkow-Blohm) reports that especially short gusts can lead to very high accelerations. In his case, a 18m gust excites the second wing bending frequency, leading to vertical accelerations at the wing tip which are a multiple of the acceleration of the overall aircraft. This is confirmed by Luber et al. [17] (Daimler Benz Aerospace), who provides the additional information that the second symmetric wing bending is at 20.33 Hz (although the publication is not clear w.r.t. the mass case). A similar finding is reported by Chapman [7] (British Aerospace, Military Aircraft Division), who states that a short gust can excite the fundamental wing bending or torsion modes, so that “parts of supersonic combat aircraft can be designed by gust induced loading rather than manoeuvre induced loads”. As these publications are from industrial companies, any quantification is missing. Also, these publications only use subsonic aerodynamic panel methods. To the author’s best knowledge, there is no publication with respect to the application of the supersonic ZONA51 panel method to the gust encounter of a complete aircraft configuration. Although this work can’t provide a full validation of the code, results will be compared taking CFD as a reference.

The aerodynamics of modern fighter configurations are slightly different compared to classical transport aircraft. Most configurations feature a vortex dominated flow, where vortices are triggered at the sharp leading edge. The DLR Future Fighter Demonstrator has a double-delta wing and is designed such that the vortices start to develop at low angles of attack and remain attached to the aircraft surface up to high angles of attack (separation starts close to $C_{l,max}$). The vortices cause high suction forces and, in this way, create additional lift on the upper surface of the aircraft, which allows for higher lift, agility and maneuverability of the aircraft. More detailed investigations of the aerodynamic characteristics are published for example by Schütte and Hummels [22] or by Zastrow et al. [32].

For the gust encounter this means that vortices are expected to develop and/or strengthen in case the gust amplitudes are sufficiently large, causing significant non-linearities as this changes the topology of the surface pressure distribution significantly. As explained above, time-linearized CFD methods usually only scale the pressure distribution and don’t capture spatial changes. Because the aircraft has a large flight envelope extending from the sub- into the supersonic regime, this leads to many different operational points. However, the benefits from both correction methods and linearized methods shrinks with an increasing number of operational points, which is due to the calculation of the time-linearized solution for many mode shapes and frequencies per operational point. Note that in this work, the focus is on two selected operational points only, but an analysis covering the whole flight envelope is planned. As a consequence, the gust encounter is simulated using CFD as a non-linear method in the time domain. To the author’s best knowledge, there is no publication on the gust encounter of a supersonic fighter aircraft using CFD methods. As the simulation of the unsteady, elastic aircraft using CFD is still computationally expensive (in this case: 2.0s gust encounter $\triangleq$ 20-40h on 128 CPUs), the Euler equations will be used, which have shown to

capture the vortex dominated flow adequately and were used by the author previously for maneuver loads analysis [30]. From Probert's overview on the wing design of combat aircraft [20], it can be concluded that much of the aerodynamic design work for the Tornado and the Eurofighter was performed using Euler codes as well. The author is fully aware that, for certain analyses, RANS simulations are mandatory and state-of-the art for many aerodynamic analyses, but the assumption is that physical effects present in the Euler solution will not vanish in a RANS analysis, on the contrary, the RANS simulation will refine the results and add more and/or new effects.

3 AEROELASTIC MODELING

The DLR Future Fighter Demonstrator (FFD) is a highly agile, two-seated aircraft with twin-engines with reheat and a targeted maximum take-off mass between 30 and 36 t. An overview of the key parameters is given in Table 1. Within the project, the DLR Institute of System Architectures in Aeronautics has taken the task to devise a conceptual design that fulfills the top level aircraft requirements (TLARs). A dedicated software and a knowledge based approach are used that relies on empirical correlations from a multitude of disciplines. They are combined with an automated constraint and mission capability analysis. More details on that approach are given by Mancini et al. [18]. The resulting conceptual design is then enhanced with a more detailed aerodynamic shape [23] in a manual step by the DLR Institute of Aerodynamics and Flow Technology. The resulting geometry of the FFD is shown in Figure 1. In parallel, an engine is designed by the DLR Institute of Propulsion Technology. To enable the exchange of information within the project, the Common Parametric Aircraft Configuration Schema (CPACS) [1] is used. For the set-up of the aeroelastic simulation models, which include the structural model, the mass models, the aerodynamic panel model, the geometry for CFD meshing, and the aero-structural coupling model, the parametric model generator ModGen [15] is used, which is developed at the DLR Institute of Aeroelasticity.

Maximum speed	VC = Ma 2.0 at 36,000 - 50,000 ft VD = Ma 2.3 at 36,000 - 50,000 ft
Maximum altitude	50,000 ft
Mission radius	550 - 700 NM
Mass	30.0 – 36.0 t maximum take-off mass (MTOM)
Payload	air 2 air mission: 1820 kg (internal) optional: 8000 kg (internal + external)
Agility	Load factor Nz = -3.0 … +9.0 with basic flight design mass (BFDM)
Longitudinal Stability	Subsonic: unstable, supersonic: stable
Control surfaces	All-movable horizontal tail planes (pitch) Ailerons along trailing edge (roll) Two vertical tail planes with rudder (yaw)

Table 1: Overview of DLR Future Fighter Demonstrator (FFD) key design parameters

3.1 Structural and Mass Modeling

The structural model must adequately represent the overall structural dynamic characteristics of the aircraft (e.g. wing bending and twist), which are important for aeroelastic analyses. Therefore, all primary structural elements, including the spars, ribs, upper and lower skin, are modeled using shell elements (CQUAD4, PSHELL and MAT1) and are completed by spar caps, stiffeners and stringers, using beam elements, to avoid local buckling and to provide a more realistic structure. For the wing, a structural layout with three main spars and multiple ribs, orientated in flow direction, is devised. Similar to the wing, the horizontal and the vertical tail are modeled and attached to the rear fuselage using rigid body elements (RBE3). Not included in the structural model are the air intakes and the cockpit. The rational behind this decision is that although both components are large, they don't belong to the primary, load-carrying structure and their influence on the overall structural dynamic behavior of the aircraft is neglected, though their mass and moment of inertia is considered. The resulting MSC.Nastran finite elements model is shown in Figure 2, has a size of ~25.000 degrees of freedom (DoF) and includes 4292 grid points, 4754 shell elements and 4096 beam elements.

The mass model includes the structural masses, system masses, fuel masses and payload. The structural masses are derived from the skin thickness and the cross section of the beam elements combined with the material density. They are completed by mass estimates for the components not included in the structural model (e.g. air intakes and cockpit). For the aircraft systems, empirical mass estimates are available from the conceptual design. In addition, a total of 9909 kg of fuel is estimated, which is distributed over four fuel tanks per side and included in the mass model with both mass and inertia properties. Finally, a design payload of 1820 kg for air to air missions is taken into account, distributed over three weapon bays. Different combinations of fuel and payload masses are considered using four mass configurations summarized in Table 2. The configurations M1 to M4 are selected in such a way that they roughly represent the different mass cases that occur during a mission of the aircraft, ranging from the heaviest mass case M1 at take-off to the lightest mass case M4 just before landing. Mass case M2 corresponds to the basic flight design mass (BFDM) where the aircraft is required to achieve its full performance. Mass case M3 is similar to M2 but without payload.

The combination of structural and mass model yields the structural dynamic properties in terms of eigenfrequencies and mode shapes. For the gust analysis, a modal reduction is applied, including the first 14 modes, which correspond to a highest frequency of 30 to 40 Hz, depending on the mass configuration. As an example, the first six mode shapes of mass configuration M2 are visualized in Figure 3. The first two elastic modes are the lateral and longitudinal fuselage bending, starting at 7.8 and 7.9 Hz for, followed by the asymmetric and

Mass case	Fuel	Payload	Mass	CG_x [m]
M1 (MTOM)	100%	Yes	26.2t	4.82
M2 (BFDM)	70%	Yes	23.2t	4.77
M3	70%	No	21.4t	4.87
M4 (OEM)	0%	No	14.5t	4.82

Table 2: Overview of mass configurations

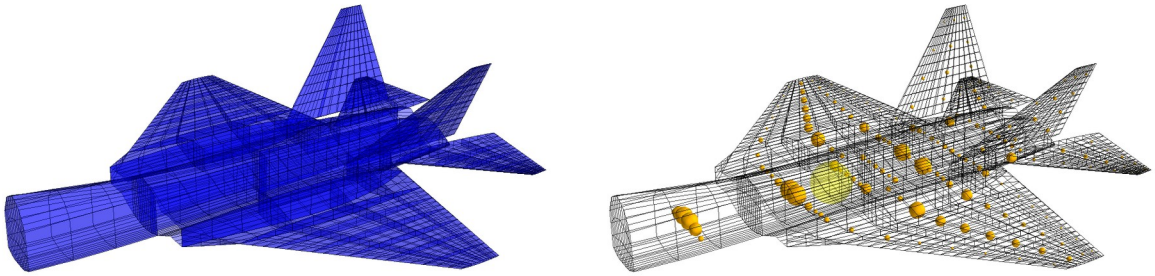

Figure 2: Structural and mass modeling

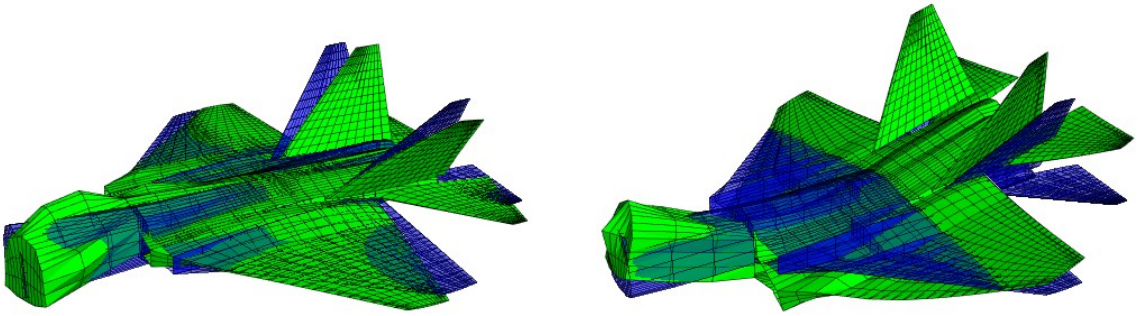

Lateral fuselage bending, 7.8 Hz

Longitudinal fuselage bending, 7.9 Hz

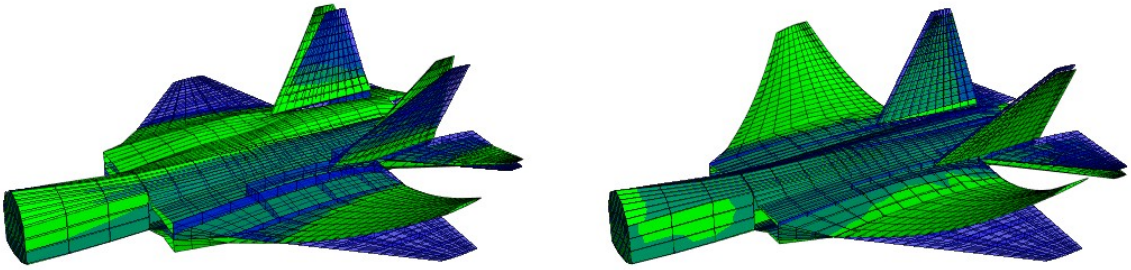

Asymmetric wing bending, 8.8 Hz

Symmetric wing bending, 9.6 Hz

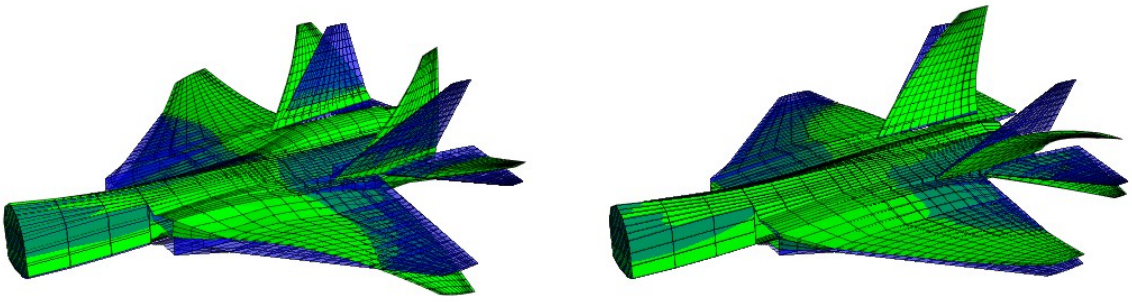

Asymmetric wing torsion, 12.7 Hz

Tail rock + asym. wing bending, 14.7 Hz

Figure 3: Overview of first elastic frequencies and mode shapes for mass configuration M2

symmetric wing bending at 8.8 and 9.6 Hz. Note that the frequencies are relatively high compared to a typical transport type aircraft, which can be explained by the stiff structure (sized to withstand maneuver load cases with a load factor Nz = -3.0 ... +9.0), the small aspect ratio as well as the large cross sections of the wing. The next mode is an asymmetric wing torsion at 12.7 Hz, followed by a tail rocking mode combined with wing bending in opposite direction at 14.7 Hz.

3.2 Aerodynamic Model

To obtain aerodynamic pressure distributions in the frequency domain, the doublet lattice method (DLM) [26] is used for the subsonic regime and the ZONA51 method [8,16] for the supersonic regime. The unsteady aerodynamics are transferred from the frequency into the time domain using a rational function approximation. For both methods, the lifting surfaces are discretized using a panel mesh shown in Figure 5. The mesh consists of 1112 panels and four control surfaces. The left and right horizontal tail planes (HTP) are all-movable while the left and right vertical tail planes (VTP) have a conventional rudder. A set of ailerons are located along the trailing edge of the main wing. Although the aerodynamic methods consider the lifting surfaces as flat plates, it is possible to add a correction for airfoil camber and wing twist, which is indicated by the color in Figure 5. Note that currently a symmetric airfoil is used for the wings, so the main influence of this correction is in the fuselage region.

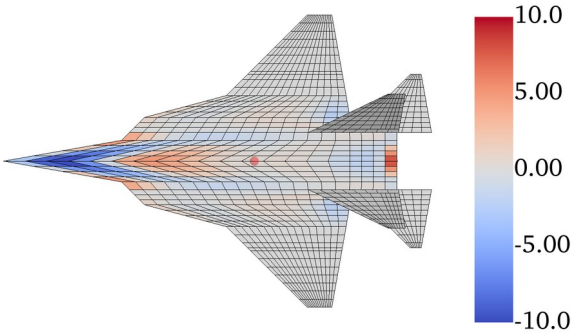

Figure 5: Aerodynamic mesh for DLM & ZONA51 incl. correction for camber and twist (indicated by color)

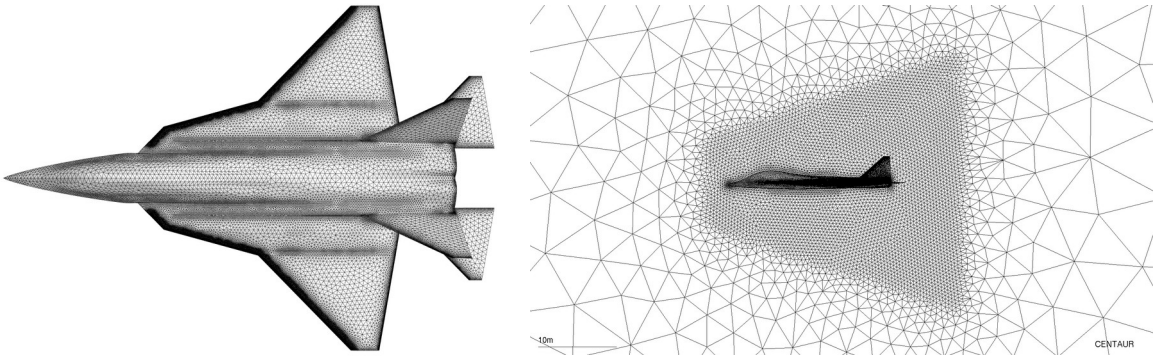

Figure 4: Aerodynamic mesh for CFD solution

The CFD mesh is generated based on the geometries generated with ModGen, which in turn uses a CPACS file as input as described above. The meshing is performed using Centaur and results in a surface mesh with ~206k triangles as shown in Figure 4 on the left. Because no boundary layer is required for Euler solutions, tetrahedrons are used to fill the spherical control volume. To better resolve vortices, which are expected already at low angles of attack, the volume mesh is refined in proximity to the aircraft using a conical frustum, visualized in Figure 4 on the right. This results in a mesh with a total number of 4.4m volume cells.

3.3 Simplified Longitudinal Flight Controller

To ensure meaningful results of the gust loads analysis, a longitudinal stability augmentation system is developed by Baier [2]. The stability augmentation system has a cascaded architecture, shown in Figure 6, which includes an attitude, pitch and actuator controller. In this way, the system allows to track a commanded pitch angle Θ or load factor N_z, depending on the flight speed of the aircraft. The individual control loops are based on a PI controller for the attitude and pitch control and a P controller for the actuator. The gains are established using a genetic algorithm which minimizes the deviation from the ideal response to pilot inputs prescribed in MIL-F-8785C. Finally, deflection rate limit filters are implemented with $\dot{\eta}_{\max} = \pm 60\ ^\circ/s$, which is selected based on comparable, current generation fighter to ensure feasible results.

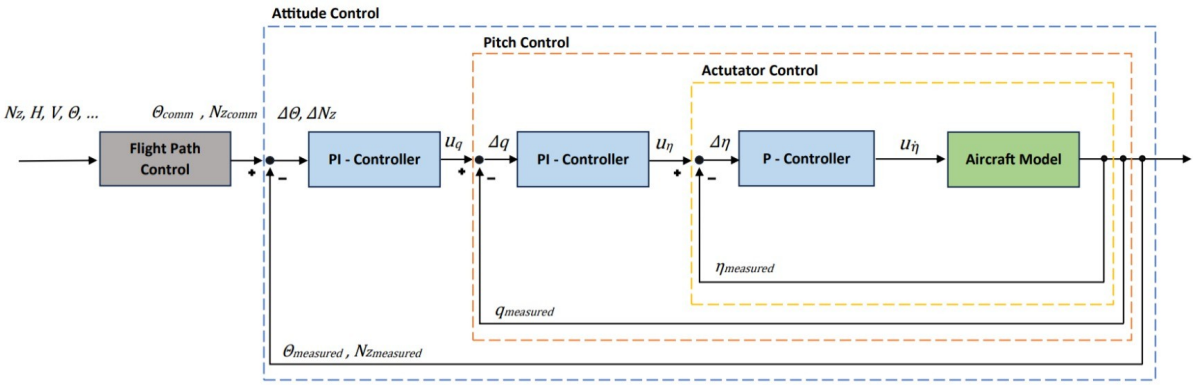

Figure 6: Proposed architecture for a simplified, longitudinal stability augmentation system [2]

3.4 Simulation Environment and Software

To capture the interaction of the elastic aircraft, the gust and the flight controller, a closed-loop time domain simulation is used. The simulation environment is based on a coupling of the loads and aeroelastic software Loads Kernel [27,28] with the CFD solver SU2 [10]. Both tools are available as open source on GitHub, see https://github.com/su2code/SU2 and https://github.com/DLR-AE/LoadsKernel. The results shown in the following sections are prepared using the software version 2023.08 and 7.5.1, respectively. The software Loads Kernel covers most types of loads and aeroelastic analyses, including maneuver, gust, landing and gyroscopic loads, flexible derivatives, control surface effectiveness, flutter, etc., based on the VLM and the DLM [26], while the CFD interface is currently available for maneuver and gust loads analysis. The two solvers are coupled in a “loose” way, which means that aerodynamic forces and surface deformations are exchanged after each time step. For the simulation of a gust in the SU2 code, the field velocity method is used, as described and

implemented by Padrón et al. [19] for 2D meshes. For this work, the existing implementation was extended to 3D meshes. In this respect, the author is very thankful for the assistance and help from the community of SU2 developers. As the name suggests, a velocity field is prescribed on every CFD grid point, which allows for differently shaped gusts in both longitudinal and lateral direction. With the field velocity method, the aircraft has no effect on the gust, but Heinrich and Reimer [13] demonstrated that this approach (called disturbance velocity approach in their work) is adequate for most practical use cases and gust lengths.

In the current approach, the onflow is prescibed using a farfield boundary condition, defined by the Mach number and an angle of attack $\alpha = 0.0°$. To capture the rigid and elastic motion of the aircraft as well as control surface deflections, the deformations of the surface mesh are calculated and handed over to the CFD solver. The CFD solver then deforms the volume mesh based on an elastic mesh approach. The aircraft can move freely within the spherical control volume, but some limitations apply, summarized in the following. During a simulation,

- the global onflow velocity and direction are constant (defined by the Mach number at the farfield),
- the density of the fluid is constant and
- only moderate flight mechanical motion w.r.t. the initial horizontal level flight is permitted (the aircraft may not leave the control volume, no excessive distortion of the CFD mesh).

As an alternative to the farfield onflow, a velocity field could be used to model the onflow, which would lift the first and last constraints. However, these limitations impose no practical constraint on the investigations of the gust encounter.

4 SUB- AND SUPERSONIC GUST ENCOUNTER

In the following, a closer look will be given on two selected operational points, the first in the subsonic regime at sea level and $Ma = 0.58$, the second within the supersonic regime at flight level FL360 and $Ma = 2.0$, highlighted by red circles in the flight envelope in Figure 7. The mass configuration is M2 (BFDM) for both cases. In the subsonic case, the rigid aircraft has a CG_x = -4.0 % MAC, indicating an unstable aircraft while in the supersonic case, the aircraft is stable with a CG_x = +14.5 % MAC. This can be explained by the large range of travel of the aerodynamic center, with a location further rearwards for supersonic speeds compared to

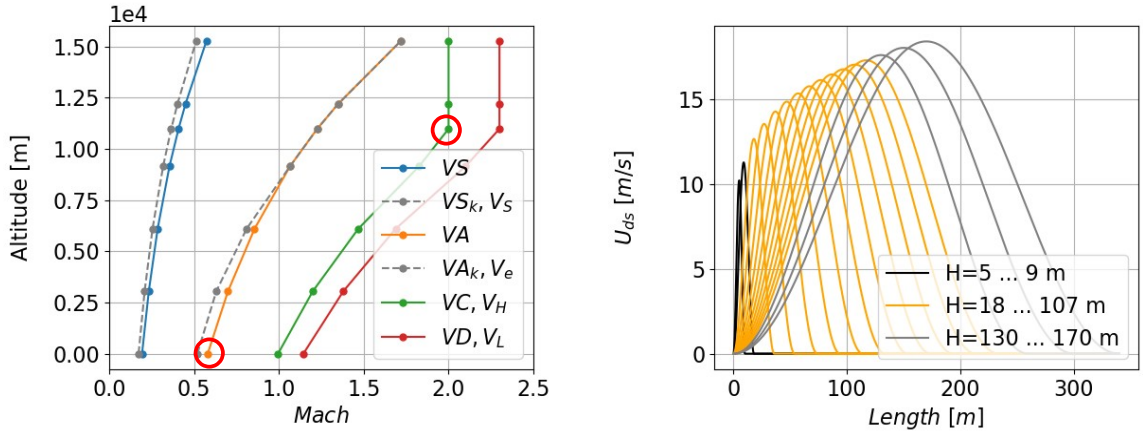

Figure 7: Flight envelope with operational points and gust velocity profiles

subsonic speeds. The gust velocities are taken from CS 25.341 but with a flight profile alleviation factor F_g = 1.0 as explained in [2,29]. In addition to the gust gradients prescribed in CS 25.341, shorter and longer gusts (up to 25 reference cord lengths) in the range of $H = 5.0 \ldots 170.0\ m$ are considered, leading to a total number of 17 vertical, upward gusts, shown in Figure 7 on the right.

4.1 Flight Mechanical Reaction During the Closed-Loop Gust Encounter

The longitudinal flight mechanical reaction of the aircraft to the gust in the subsonic regime is shown in Figure 8. Comparing the curves based on panel methods (given in blue color, left side) with those based on CFD methods (given in green color, right side), the results look very similar at a first glance. All simulations start in a trimmed, horizontal level flight, in this case with an angle of attack $\alpha_{\mathrm{DLM}} \approx 1.9°$ and $\alpha_{\mathrm{CFD}} \approx 2.1°$. The highest angles of attack are reached for moderate gust lengths with $\alpha_{\mathrm{DLM}} \approx 6.1°$ and $\alpha_{\mathrm{CFD}} \approx 6.6°$ and with a more pronounced plateau for the CFD methods. This is because with CFD, the initial pitch-up of the aircraft is greater, as can be seen on the basis of the pitch rate q and the pitch angle Θ, while the heave motion is similar as indicated by the vertical velocity w. The control surface command η shows the largest differences with initial values $\eta_{\mathrm{DLM}} \approx 0.7°$ and $\eta_{\mathrm{CFD}} \approx 2.7°$. This indicates a slightly different aerodynamic pitching moment of the aircraft, which can be explained by the modeling of the volumetric fuselage in CFD while for the DLM and

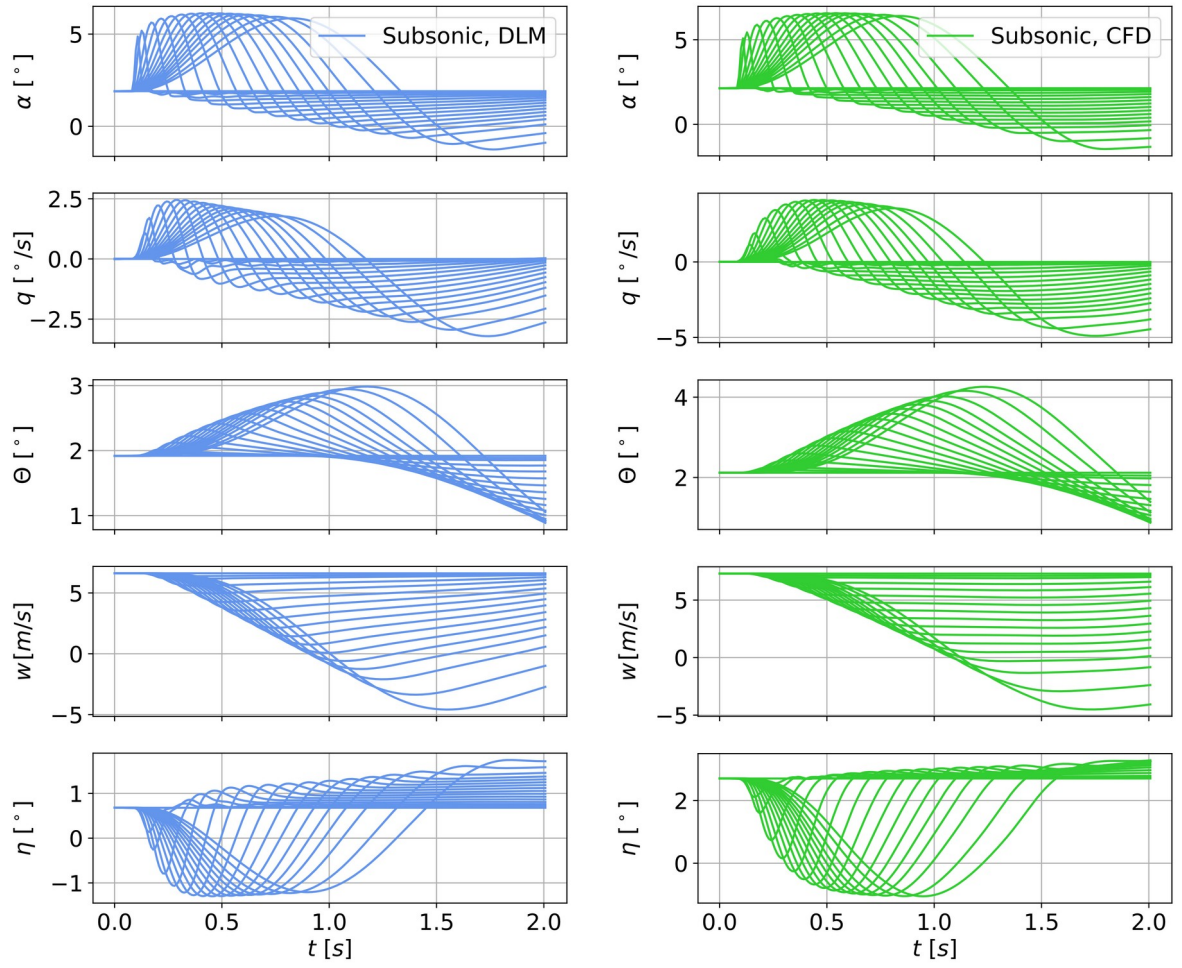

Figure 8: Flight mechanical reaction during the subsonic, closed-loop gust encounter

ZONA51, the flat plate approach used. In that way, the fuselage is modeled like a wing, and the correction for camber and twist is obviously not perfect. In addition to this initial offset and as a consequence of the higher pitch rate q and the pitch angle Θ, the flight controller also commands higher deflections of the horizontal tail plane in CFD with $\Delta\eta_{\mathrm{CFD}} \approx 3.8°$ compared to $\Delta\eta_{\mathrm{DLM}} \approx 2.0°$.

The results for the supersonic regime are presented in Figure 9. Overall, the agreement of the curves is better compared to the subsonic regime. However, now the panel method ZONA51 yields slightly higher pitch rates q, pitch angles Θ and higher deflections $\Delta\eta$ of the horizontal tail when compared to CFD. Overall, the increase of the angle of attack α is much smaller, which can be explained by the high flight speed in relation to the amplitudes to the gusts. Still, as the dynamic pressure q_∞ is multiple times higher compared to the subsonic regime, small angles of attack may cause high aerodynamic forces as will be shown in Section 4.3.

With respect to the longitudinal flight controller, it can be concluded that the design presented in Section 3.3 immediately reacts to the gust encounter and stabilized the aircraft reliably for both the aerodynamic panel methods and well as for CFD methods, although the parameters of the controller were defined based on panel methods only.

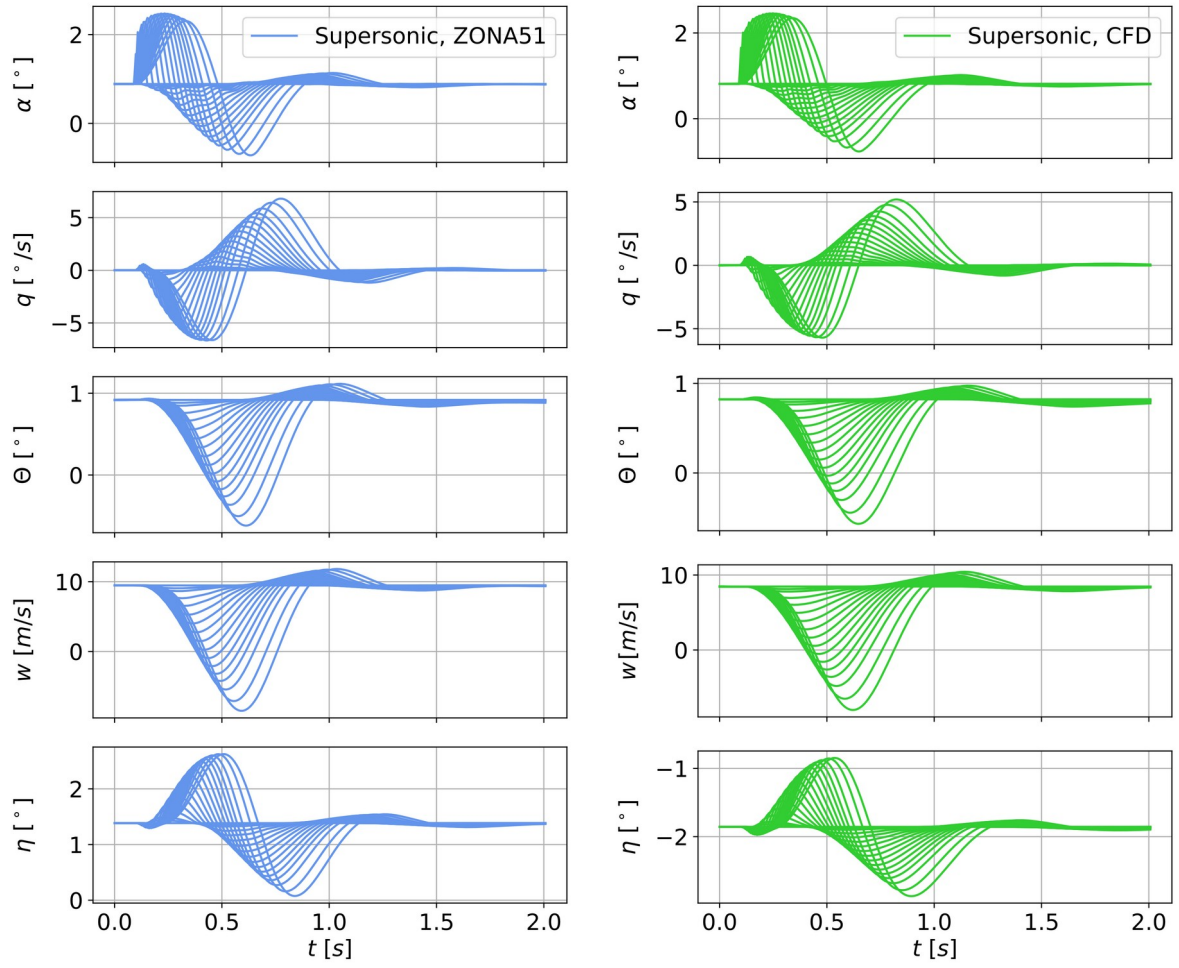

Figure 9: Flight mechanical reaction during the supersonic, closed-loop gust encounter

4.2 Aerodynamic Non-Linearities due to Vortex Build-Up

The changes in the angles of attack observed in the previous section are sufficiently large for vortices to develop during a gust encounter, which is shown in the following. To get a better understanding, the surface and volume solution of one exemplary subsonic gust encounter with a gust gradient $H = 97m$ is analyzed. Figures 10 and 11 show a visualization of the vortices using the Q-criterion [3,9] with iso-surfaces at $Q = 50$ as well as the distribution of the pressure coefficients c_p on the aircraft surface at three different time steps. In addition, the vertical grid velocity is shown in blue to red colors by slicing vertically through the volume solution at the center plane.

At t=0.27s the gust has just reached the aircraft, as can be seen by the light-blue color on the left side of the plot. The Q-criterion already shows multiple regions of rotation-dominated flow, for example at the sharp leading edges of the wing, the strake and the tail, at the chine (sharp edge at the aircraft nose) and at the wing tips, but no “true” primary vortices. The pressure distribution is rather smooth (yellow to orange colors) and shows a pronounced suction peak (yellow to green colors) at the leading edges of the main wing and the strake.

At t=0.38s the aircraft has penetrated deeper into the gust and the strake vortex starts to develop, which is also visible in the pressure distribution where the color changes from orange to yellow in the area of the vortex.

At t=0.63s the aircraft is in the middle of the gust and both the strake and the wing vortices are visible and leave a clear “footprint” in the surface pressure distribution in terms of high suction forces, indicated by the green colors. For a better quantification, the pressure coefficient c_p is given for one selected section of the wing in the top left corner of each figure. One can clearly see the peak caused by the wing vortex at t=0.67s, while at t=0.27s there is simply a normal, subsonic suction peak at the leading edge.

Although the angles of attack during the gust encounter are moderate with $\alpha_{\mathrm{CFD}} \approx 6.6^{\circ}$, this is already sufficient to cause significant non-linearities on the aerodynamic side and significant changes to the topology of the surface pressure distribution. As mentioned in the introduction, such spatial changes wouldn’t be resolved by time-linearized CFD methods. Also remember that the aerodynamic panel methods don’t capture this kind of vortices at all. Consequently, the gust loads acting on the aircraft are different, which is investigated in the next section. In addition, the strong suction peak of the strake vortex may contribute to the initial pitch-up motion of the aircraft as that area is located in front of the center of gravity, which in turn influences the gust loads.

During the supersonic gust encounter, the changes of the angle of attack are smaller and no vortices could be observed. However, one single supersonic operational point is not representative and vortices might occur in different areas of the flight envelope as well.

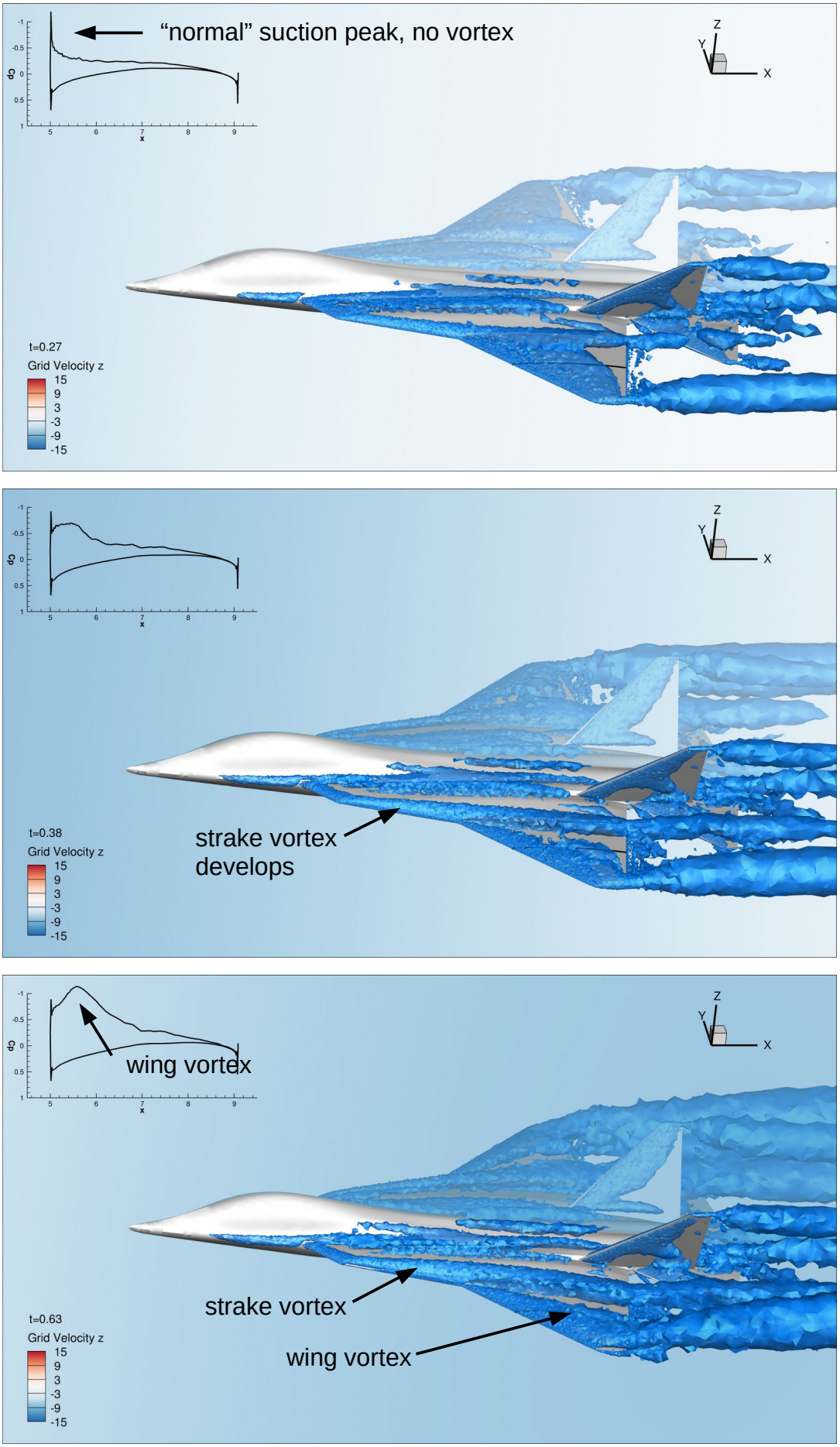

Figures 10: Vortex development during subsonic gust encounter at t=0.27s, t=0.68s and t=0.63s

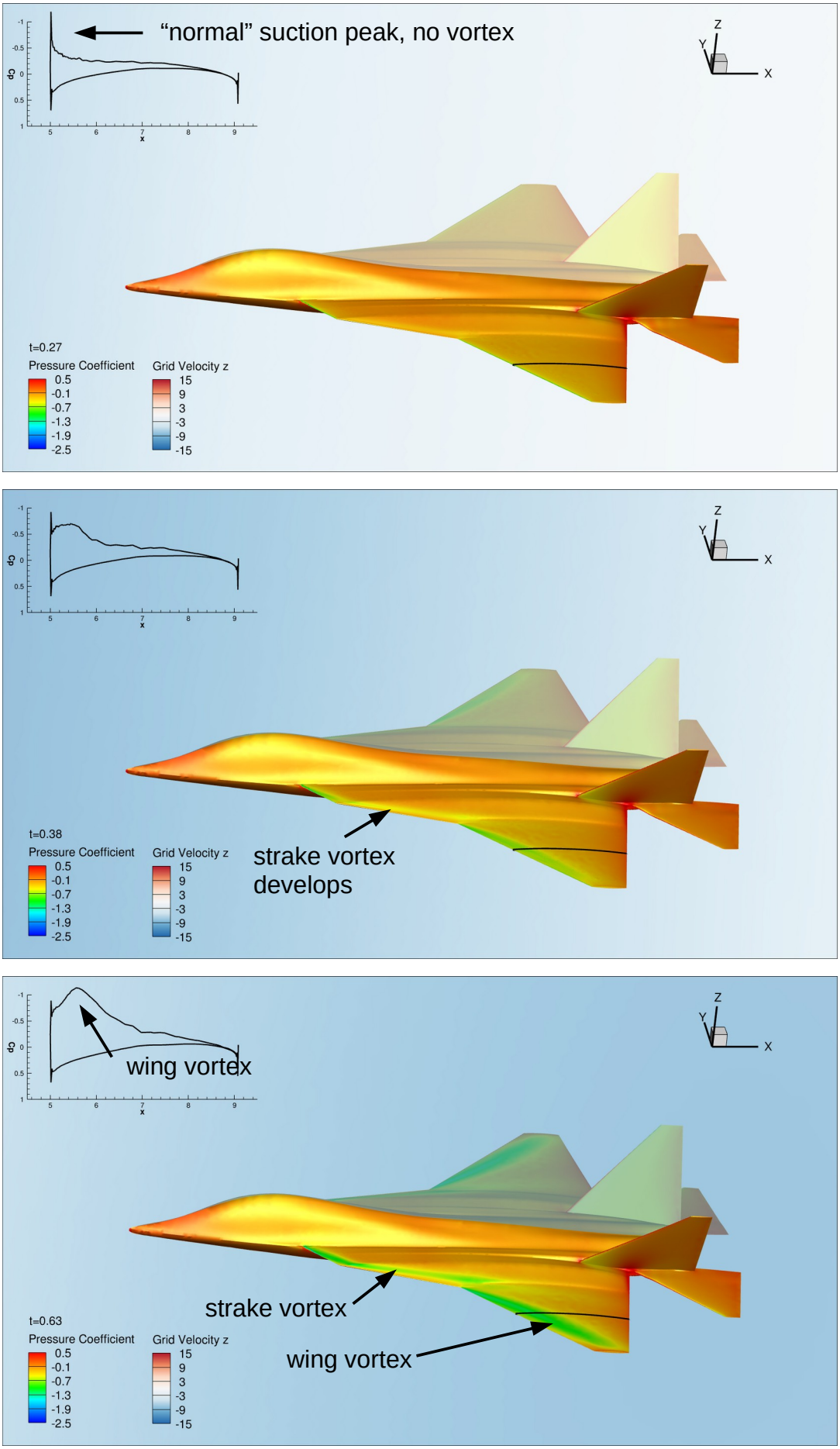

Figures 11: Pressure distribution during subsonic gust encounter at t=0.27s, t=0.68s and t=0.63s

4.3 Quantification of Section Loads

The section loads are quantified in terms of wing root bending and torsion moments M_x and M_y and illustrated using the same color scheme as above - panel methods in blue, CFD in green. The results for the subsonic gust encounter are given in Figure 12 and start from a trimmed, horizontal level flight. Looking at the wing root bending moment M_x, the maximum values are $M_x^{\mathrm{DLM}} \approx 4.0 \cdot 10^5$ and $M_x^{\mathrm{CFD}} \approx 4.7 \cdot 10^5$. Subtracting the initial values, the incremental ΔM_x during the gust encounter differs by 25%. This difference can be explained by to the vortex build-up analyzed in Section 4.2, creating significant suction peaks on the aircraft surface and thus increasing both the lift and the wing root bending moments M_x. For the wing root torsion moments M_y, the differences are even more pronounced. For DLM, the maximal values are $M_y^{\mathrm{DLM}} \approx 2.2 \cdot 10^5$ compared to $M_y^{\mathrm{CFD}} \approx 3.3 \cdot 10^5$. Subtracting the initial values, this leads to an increase of about 60 % in the incremental ΔM_y using CFD. This is because the additional suction peaks create a nose-up torsion moment M_y. Note that for the

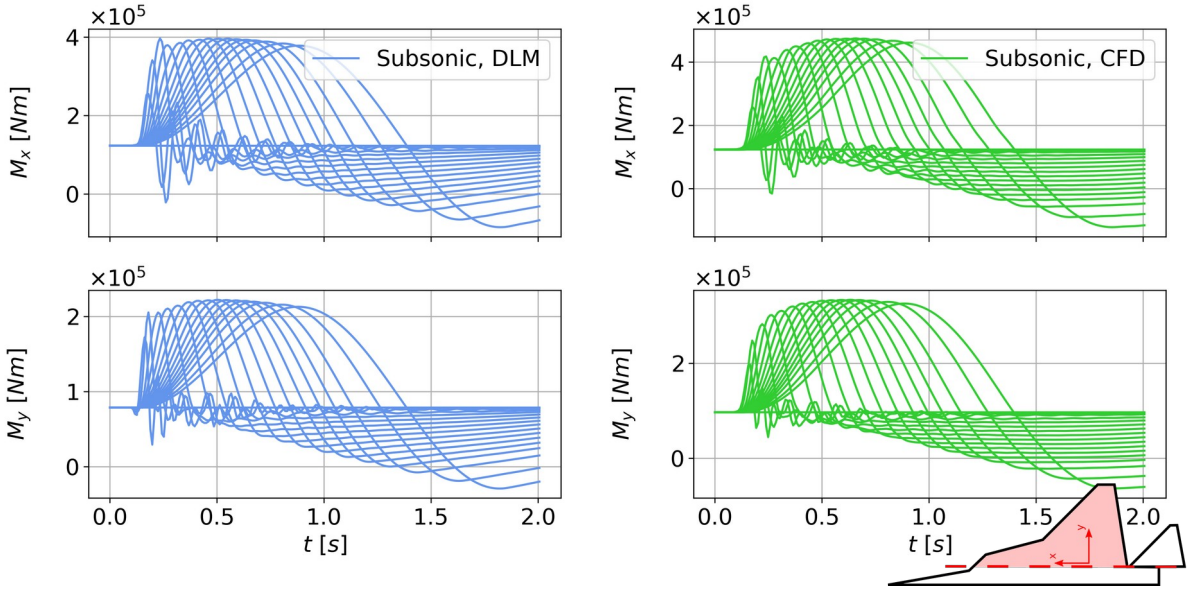

Figure 12: Bending and torsion moments at the wing root during the subsonic, closed-loop gust encounter

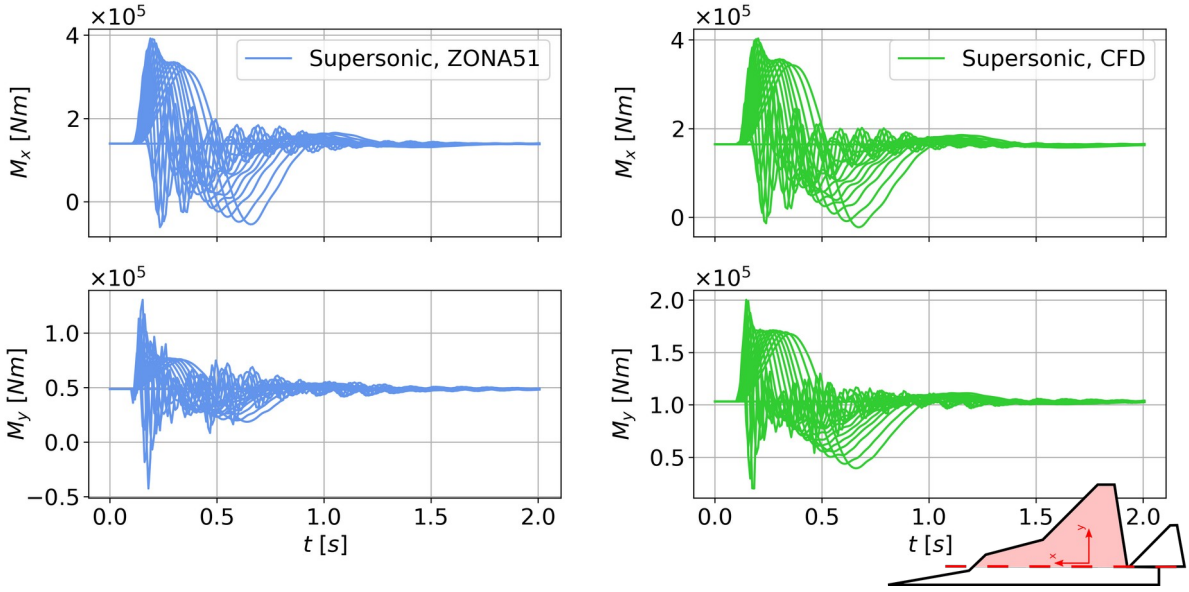

Figure 13: Bending and torsion moments at the wing root during the supersonic, closed-loop gust encounter

torsion moments M_y, the magnitude also depends on the location and orientation of the monitoring station. Concerning the "worst" gust, in this operational point the highest loads occur for a gust gradient $H = 77m$ for DLM and $H = 107m$ with CFD, although in the range $H = 77m \ldots 127m$ the results are close to each other.

For conventional transport aircraft, capturing the span-wise elastic twist and the resulting lift distribution is the driving factor for correct wing root section loads and non-linearities due to shock-induced separation or shock motion may have an influence in some cases. For the FFD configuration, capturing the vortices appears to be the key for reliable gust loads.

The section loads in the supersonic regime are shown in Figure 13. Looking at the wing root bending and torsion moments M_x and M_y, the loads due to short gusts in the range of $H = 27 \ldots 77\ m$ are significantly higher compared to the other gust lengths. This is due to an excitation of structural dynamic modes, which are shown in Figure 14. The upper plot shows the time histories of the generalized coordinate of selected modes during a gust with $H = 37\ m$ while the lower plot shows a gust with $H = 107\ m$. For both the ZONA51 and CFD method, a strong reaction of the first symmetric wing bending and the longitudinal fuselage bending modes can be seen for $H = 37\ m$ while there is nearly no visible change for $H = 107\ m$. This shows the necessity of a transient gust analysis for fighter aircraft that includes structural elasticity - a steady approach with a rigid aircraft, for example using the Pratt formula, would miss these effects.

To answer the question whether gusts in the sub- or the supersonic regime are more important, an analysis based on aerodynamic panel methods that covers the whole flight envelope will be presented in [29].

5 SUMMARY AND OUTLOOK

A previous work [30] showed that for maneuver loads, aerodynamic panel methods are at their physical limit and that in particular for fighter aircraft, CFD should be preferred over panel methods. This work investigates gust loads. The comparisons reveal only moderate agreement between aerodynamic panel methods and CFD.

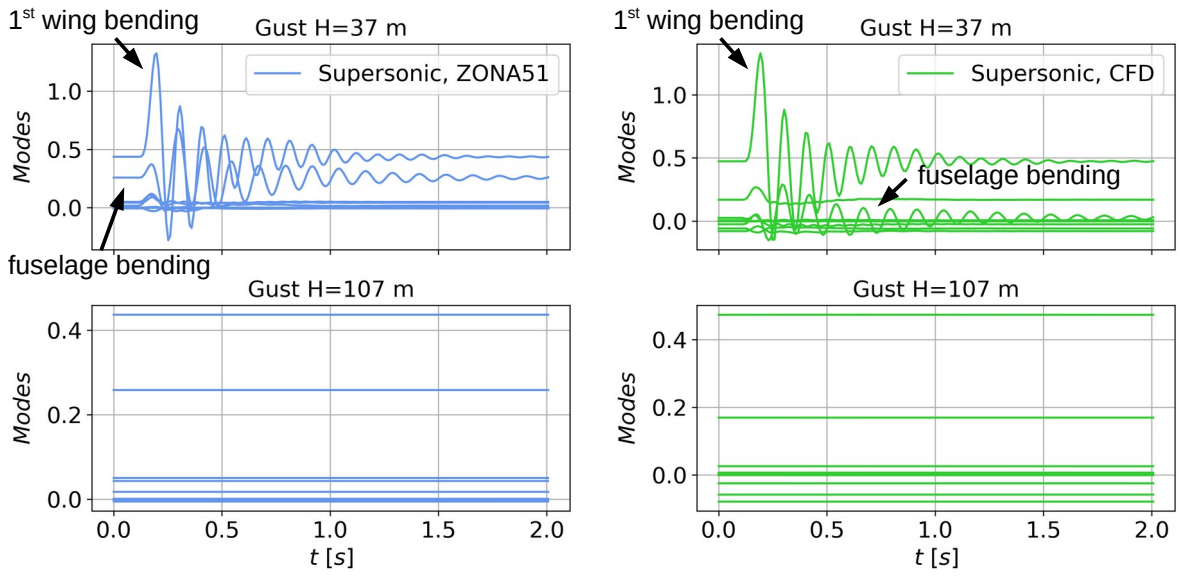

Figure 14: Excitation of structural modes during the supersonic, closed-loop gust encounter

This has multiple reasons: the two aerodynamic methods yield different aerodynamic centers and pitching moments, effecting the longitudinal motion and the initial trim condition of the aircraft. A correction for camber and twist was applied but is not sufficient - capturing these effects would require a more elaborate correction, e.g. of the lift gradients. This has an influence on the flight mechanical reaction of the aircraft, including different reactions of the flight controller. Due to the increase of the effective angle of attack, vortices develop during the gust encounter, which were not present in horizontal level flight. Because of the large suction peaks due to the vortices, the topology of the surface pressure distribution changes significantly. These effects are missed completely by the aerodynamic panel methods. Ultimately, this leads to differences in section loads, which are higher using CFD. It is also shown that for fighter aircraft, a transient gust analysis including structural elasticity is necessary, confirming and quantifying the findings of previous authors.

The following points remain open and require further research. Answering the first two point (at least partially) is planned in a next publication [29].

- Investigation of the whole flight envelope (about 4000 gust simulations) to find the highest loads and to classify gust loads with respect to maneuver loads.
- Quantification of local accelerations due to the structural dynamic response, for example at the wing tip.
- Superposition of gust and maneuver loads, as some specifications suggest.

ACKNOWLEDGMENTS

The author would like to thank the community of SU2 developers for their help and assistance.

REFERENCES

[1] Alder, M., Moerland, E., Jepsen, J., and Nagel, B., “Recent Advances in Establishing a Common Language for Aircraft Design with CPACS,” presented at the Aerospace Europe Conference 2020, Bordeaux, Frankreich, 2020, https://elib.dlr.de/134341/.

[2] Baier, J., “Gust Load Prediction on Supersonic Future Fighter Aircraft,” Bachelor Thesis, TU München & DLR Institute of Aeroelasticity, Göttingen, Germany, 2023.

[3] Banko, A. J., and Eaton, J. K., “A frame-invariant definition of the Q-criterion,” *Stanford University Center for Turbulence Research Annual Research Briefs*, pp. 181–194, 2019.

[4] Becker, J., “Gust Load Prediction and Alleviation on a Fighter Aircraft,” AGARD Structures and Materials Panel, Oberammergau, Germany, AGARD Report No.728, Sep. 1985.

[5] Bekemeyer, P., Ripepi, M., Heinrich, R., and Görtz, S., “Nonlinear Unsteady Reduced-Order Modeling for Gust-Load Predictions,” *AIAA Journal*, vol. 57, no. 5, pp. 1839–1850, May 2019, https://doi.org/10.2514/1.J057804.

[6] Bekemeyer, P., Thormann, R., and Timme, S., “Frequency-Domain Gust Response Simulation Using Computational Fluid Dynamics,” *AIAA Journal*, vol. 55, no. 7, pp. 2174–2185, Jul. 2017, https://doi.org/10.2514/1.J055373.

[7] Chapman, R., “Dynamic Loading Considerations in Design of Modern Combat Aircraft,” presented at the AGARD Structures and Materials Panel meeting on “Loads and Requirements for Military Aircraft,” Florence, Italy, 1996.

[8] Chen, P.-C., and Liu, D. D., “A harmonic gradient method for unsteady supersonic flow calculations,” *Journal of Aircraft*, vol. 22, no. 5, pp. 371–379, 1985, https://doi.org/10.2514/3.45134.

[9] Chong, M. S., Perry, A. E., and Cantwell, B. J., “A general classification of three-dimensional flow fields,” *Physics of Fluids A: Fluid Dynamics*, vol. 2, no. 5, pp. 765–777, May 1990, https://doi.org/10.1063/1.857730.

[10] Economon, T. D., Palacios, F., Copeland, S. R., Lukaczyk, T. W., and Alonso, J. J., “SU2: An Open-Source Suite for Multiphysics Simulation and Design,” *AIAA Journal*, vol. 54, no. 3, pp. 828–846, März 2016, https://doi.org/10.2514/1.J053813.

[11] Friedewald, D., “Large-Amplitude Gusts on the NASA Common Research Model,” *Journal of Aircraft*, pp. 1–16, Jun. 2023, https://doi.org/10.2514/1.C037198.

[12] Friedewald, D., “Numerical Simulations on Unsteady Nonlinear Transonic Airfoil Flow,” *Aerospace*, vol. 8, no. 1, pp. 1–25, Dec. 2020, https://www.mdpi.com/2226-4310/8/1/7.

[13] Heinrich, R., and Reimer, L., “Comparison of different approaches for gust modeling in the CFD Code TAU,” presented at the International Forum on Aeroelasticity & Structural Dynamics 2013, Bristol, Großbritannien, 2013, http://elib.dlr.de/85834/.

[14] Kaiser, C., and Quero Martin, D., “Quantification of nonlinear effects in gust load prediction,” presented at the 18th International Forum on Aeroelasticity and Structural Dynamics, Savannah, Georgia, 2019.

[15] Klimmek, T., “Parameterization of topology and geometry for the multidisciplinary optimization of wing structures,” in *CEAS 2009 - European Air and Space Conference*, Manchester, United Kingdom, 2009.

[16] Liu, D. D., James, D. K., Chen, P. C., and Pototzky, A. S., “Further studies of harmonic gradient method for supersonic aeroelastic applications,” *Journal of Aircraft*, vol. 28, no. 9, pp. 598–605, 1991, https://doi.org/10.2514/3.46070.

[17] Luber, Wolfgang G., Becker, J., and Sensburg, O., “The Impact of Dynamic Loads on the Design of Military Aircraft,” presented at the AGARD Structures and Materials Panel meeting on “Loads and Requirements for Military Aircraft,” Florence, Italy, 1996.

[18] Mancini, A., Zamboni, J., and Moerland, E., “A Knowledge-based Methodology for the Initiation of Military Aircraft Configurations,” presented at the AIAA AVIATION 2021 FORUM, Virtual Event, 2021, https://doi.org/10.2514/6.2021-2789.

[19] Padron, A. S., Alonso, J. J., Palacios, F., Barone, M. F., and Eldred, M. S., “Multi-Fidelity Uncertainty Quantification: Application to a Vertical Axis Wind Turbine Under an Extreme Gust,” in *15th AIAA/ISSMO Multidisciplinary Analysis and Optimization Conference*, 2014, https://doi.org/10.2514/6.2014-3013.

[20] Probert, B., “Aspects of Wing Design for Transonic and Supersonic Combat Aircraft,” presented at the RTO AVT Course on “Fluid Dynamics Research on Supersonic Aircraft,” Rhode-Saint-Gentèse, Belgium, 1998.

[21] Quero Martin, D., “An Aeroelastic Reduced Order Model for Dynamic Response Prediction to Gust Encounters,” Dissertation, TU Berlin, Berlin, 2016.

[22] Schütte, A., and Hummel, D., “Numerical Design Studies on the Roll Stability of a Multi-Delta-Wing Configuration,” *Journal of Aircraft*, vol. 60, no. 3, pp. 898–914, May 2023, https://doi.org/10.2514/1.C037128.

[23] Stradtner, M., Liersch, C. M., and Löchert, P., “Multi-Fidelity Aerodynamic Data Set Generation for Early Aircraft Design Phases,” presented at the AVT-366 Use of Computational Fluid Dynamics for Design and Analysis: Bridging the Gap Between Industry and Developers, 2022.

[24] Vidy, C., Förster, M., Iatrou, M., and Breitsamer, C., “Dynamic Stability and Response Analysis Using a Small-Disturbance CFD Method,” presented at the International Forum for Aeroelasticity and Structural Dynamics, Bristol, 2013.

[25] Vidy, C., Katzenmeier, L., Winter, M., and Breitsamer, C., “Verification of the use of small-disturbance CFD aerodynamics in flutter and gust analyses for simple to highly complex configurations,” presented at the International Forum for Aeroelasticity and Structural Dynamics, Saint Petersburg, Russia, 2015.
[26] Voß, A., “An Implementation of the Vortex Lattice and the Doublet Lattice Method,” Institut für Aeroelastik, Deutsches Zentrum für Luft- und Raumfahrt, Göttingen, Germany, Technical Report DLR-IB-AE-GO-2020-137, Oktober 2020, https://elib.dlr.de/136536/.
[27] Voß, A., “DLR-AE/LoadsKernel,” https://doi.org/10.5281/zenodo.8341566.
[28] Voß, A., “Loads Kernel User Guide,” Institut für Aeroelastik, Deutsches Zentrum für Luft- und Raumfahrt, Göttingen, Germany, Technical Report DLR-IB-AE-GO-2020-136, Jul. 2020, https://elib.dlr.de/140268/.
[29] Voß, A., and Baier, J., “Closed-Loop Gust Loads Analysis of a Fighter Aircraft,” presented at the 34th Congress of the International Council of the Aeronautical Sciences, Florence, Italy, 2024.
[30] Voß, A., and Klimmek, T., “Parametric aeroelastic modeling, maneuver loads analysis using CFD methods and structural design of a fighter aircraft,” *Aerospace Science and Technology*, vol. 136, Mar. 2023, https://doi.org/10.1016/j.ast.2023.108231.
[31] Weigold, W., Stickan, B., Travieso-Alvarez, I., Kaiser, C., and Teufel, P., “Linearized Unsteady CFD for Gust Loads with TAU,” in *IFASD 2017 - 17th International Forum on Aeroelasticity and Structural Dynamics*, Como, Italy, 2017.
[32] Zastrow, J., Oberdieck, F., Henne, U., and Klein, C., “Numerical and Experimental Investigations on the DLR-F23 Combat Aircraft Wind Tunnel Model,” presented at the ICAS Congress, Stockholm, Sweden, 2022.

COPYRIGHT STATEMENT